Journal Name

ARTICLE TYPE

Cite this: DOI: 00.0000/xxxxxxxxxx

$Yb_5Rh_6Sn_{18}$: a valence fluctuating system with ultra-low thermal conductivity

Oleksandr Bolielyi,[a] Volodymyr Levytskyi,[a] Jörg Wagler,[b] Kristina O. Kvashnina,[c,d] Bohdan Kundys,[e] Andreas Leithe-Jasper[f] and Roman Gumeniuk*[a]

Received Date
Accepted Date

DOI: 00.0000/xxxxxxxxxx

1 Supporting Information

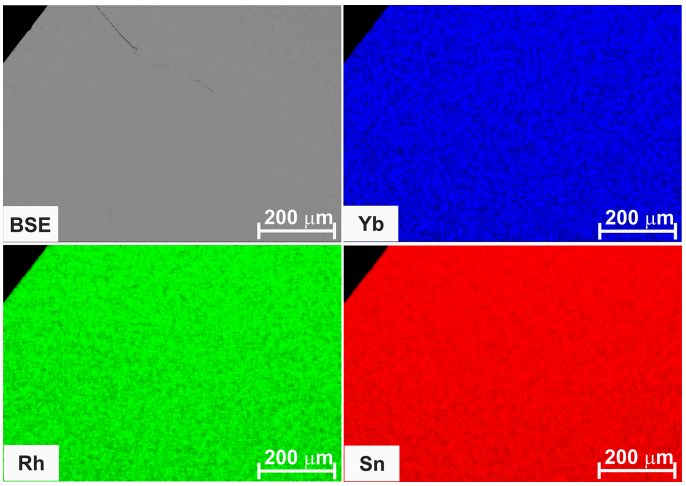

Fig. S1 SEM picture of selected polished surface of the $Yb_5Rh_6Sn_{18}$ sample together with X-ray intensity element mappings and corresponding EDXS absolute counts of YbL_α, RhL_α and SnL_α lines.

1.1 Interconfigurational fluctuation model (ICF)

The ICF model assumes two energetic states are corresponding to certain valences and thus, describes the difference between them as an interconfigurational excitation energy (E_{ex}).[1] Within such a description, the fractional occupation of the divalent state is given as:

$$\nu_{eff} = \frac{1}{1+8\exp[-E_{ex}/k_B(T+T_{sf})]} \quad (1)$$

where, T_{sf} is staying for the width of sublevels of corresponding configurations. Hence, the temperature dependence of magnetic susceptibility of a intermediate valence system can be described as:

$$\chi_{ICF}(T) = \frac{N_A\mu_{eff}^2}{3k_B}\frac{1-\nu_{eff}}{(T+T_{sf})} \quad (2)$$

Obviously, since almost all studied intermetallics are contami-

[a] Institut für Experimentelle Physik, TU Bergakademie Freiberg, Leipziger Straße 23, 09596 Freiberg, Germany; E-mail: roman.gumeniuk@physik.tu-freiberg.de
[b] Institut für Anorganische Chemie, TU Bergakademie Freiberg, Leipziger Straße 29, 09599 Freiberg, Germany
[c] The Rossendorf Beamline at ESRF, CS 40220, 38043 Grenoble Cedex 9, France
[d] Helmholtz-Zentrum Dresden-Rossendorf (HZDR), Institute of Resource Ecology, P.O. Box 510119, 01314 Dresden, Germany
[e] Université de Strasbourg, CNRS, Institut de Physique et Chimie des Matériaux de Strasbourg, UMR 7504, Strasbourg F-67000, France
[f] Max-Planck-Institut für Chemische Physik fester Stoffe, Nöthnitzer Straße 40, 01187 Dresden, Germany

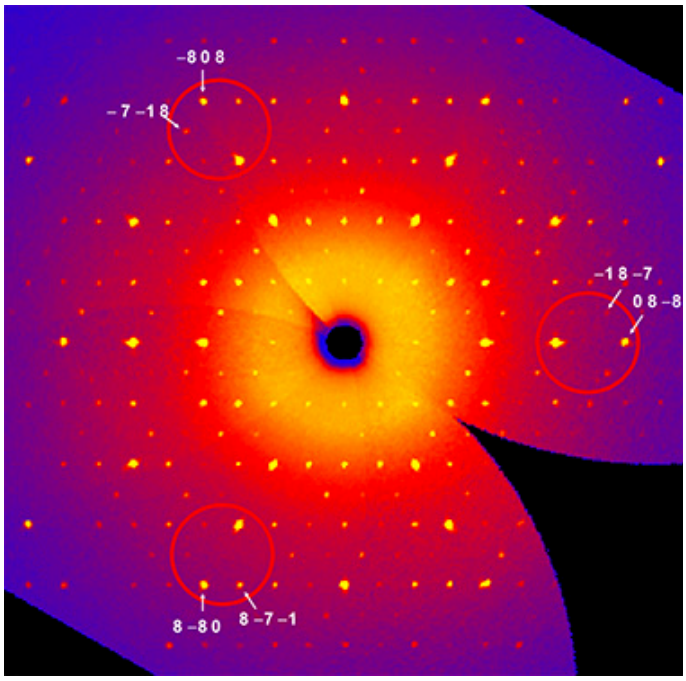

Fig. S2 Simulated rotation about (1 1 1) for the cubic cell setting, generated from the Image Plate collected data. Whereas the strongest reflections represent a cubic pattern [shown for the set (0 8 -8), (8 -8 0), (-8 0 8)], adjacent weaker reflections show noticeable deviations from symmetry equivalence [shown for the set (-1 8 -7), (8 -7 -1), (-7 -1 8)]

nated by minor paramagnetic impurities (cannot be avoided because of impure elements used for the syntheses) as well as by the contributions of conduction electrons, Eq. S2 needs to be corrected by the $\chi_{\rm imp}(T) = C_{\rm imp}/(T-\Theta_{\rm imp})$ and χ_0 contributions, respectively. Hence, the final model, which can be used for a fit is the following:

$$\chi(T) = \chi_{\rm ICF}(T) + \chi_{\rm imp}(T) + \chi_0 \qquad (3)$$

Fitting $\chi(T)$ of $Yb_5Rh_6Sn_{18}$ to Eq. S3 (Fig. S3), we obtain: $E_{\rm ex}/k_{\rm B} = 268.4(9)$ K; $T_{\rm sf} = 38.3(4)$ K; $C_{\rm imp} = 0.8(2)$ emu K mol^{-1}; $\Theta_{\rm imp} = 36.9(2)$ K and $\chi_0 = 3.1(5)\times10^{-3}$ emu mol^{-1}. Having now the $C_{\rm imp}$ value, the percentage of impurities originating from unquenched Yb^{3+}-ions are calculated as $n_{\rm imp} = C_{\rm imp}/C_{\rm Yb^{3+}} = 6.2$ at. % per mole of $Yb_5Rh_6Sn_{18}$ [with $C_{\rm Yb^{3+}} = 5(\mu^2_{\rm eff}/8)$].[2] The latter number seems to be enhanced, which can be also related to the poor description by ICF-model of the low- ($T < 50$ K) (inset b of Fig. S2) and high-temperature ($T > 250$ K) regions of $\chi(T)$ of $Yb_5Rh_6Sn_{18}$ (Fig. S2). The spin fluctuation temperature $T_{\rm sf} = 38.3(4)$ K is by a factor of ≈6 smaller then the value of T_0 obtained from BCW model. Similar relations between these parameters are reported for $Yb_3Co_4Ge_{13}$ Remeika phase[3] and $YbPtGe_2$[4].

Further, the average valence of Yb atoms in $Yb_5Rh_6Sn_{18}$ was calculated from $n^+ = 2\nu_{\rm eff} + 3(1-\nu_{\rm eff})$. As one can see from the inset a to Fig. S2, the amplitude of the change of ICF valence is much larger in comparison to that observed from X-ray absorption spectra. Actually, the failure of a simplified two-level model accounting neither for the whole multiplets, nor for CEF effects nor for Kondo interactions, in the description of $n^+(T)$ for such a

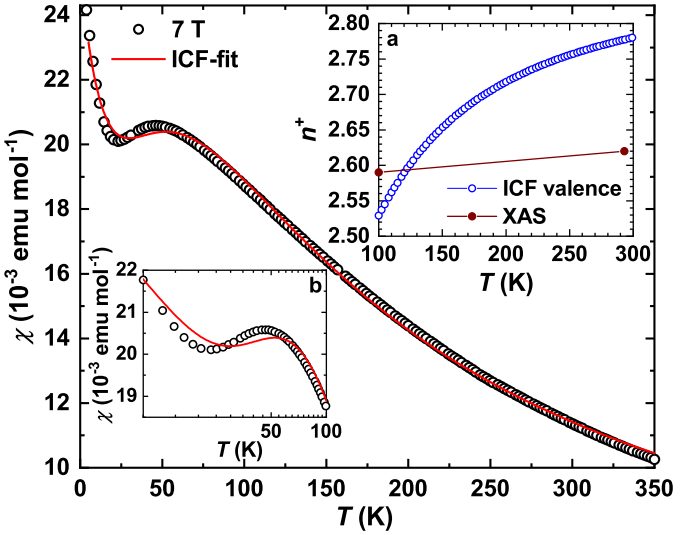

Fig. S3 Temperature dependence of magnetic susceptibility of $Yb_5Rh_6Sn_{18}$ together with the fit to ICF-model. Inset a: Temperature dependencies of Yb-valences deduced from ICF-model in comparison with the experimetal values obtained from XAS. Inset b: $\chi(T)$ together with ICF-fit in low temperature range.

complex system as $Yb_5Rh_6Sn_{18}$ could be expected.

Our observation is justified by investigations performed on YbCuAl[5] and YbB_{12}[6], for which the splitting energy between the $J = 7/2$ ground state and $J = 5/2$ excited state for Yb^{3+}-ions is of huge ~ 1.3 eV value. The simulation of the latter is a true challenge even for quantum-mechanical models. For all these reasons ICF normally fails in the description of valence fluctuations in Ce- and Yb-containing intermetallics.

1.2 Electrical resistivity with Bloch-Grüneisen description

Electrical resistivity of $Yb_5Rh_6Sn_{18}$ for $3\,{\rm K} < T < 40\,{\rm K}$ can be described with the Bloch-Grüneisen (BG) formula assuming domination of the *s-d* interband scattering mechanism (i.e., $n = 3$)[7]:

$$\rho(T) = \rho_0 + A\left(\frac{T}{\Theta_{\rm D}^{\rm res}}\right)^n \int_0^{\Theta_{\rm D}^{\rm res}/T} \frac{x^n}{(e^x-1)(1-e^{-x})}dx \qquad (4)$$

where residual resistivity ρ_0 denotes the scattering on defects, A is a coefficient depending on the phonon contribution and $\Theta_{\rm D}^{\rm res}$ stays for the characteristic Debye temperature. The parameters obtained from such a fit are collected in Table S1. The fact that BG formula works is in agreement with a strong relevance of electron-electron scattering, which is reflected in a $\rho \sim T^2$ behavior discussed in the main text.

At $T \approx 50$ K, $\rho(T)$ of $Yb_5Rh_6Sn_{18}$ deviates from BG formula with $n = 3$-like behavior, shows a rounding and for $T > 100$ K fits well to Eq. 4 with $n = 2$, thus indicating the electron-electron scattering mechanism to become a dominant one. Such a switch would be in line with increasing of Yb-valence with temperature (i.e., slight increase of charge carrier concentration.)

As one can see from Table S1, the $\Theta_{\rm D}^{\rm res}$ values obtained from both fits are nearly the same, which confirms that the BG model only accounts for electron scattering on longitudinal acoustic phonons[8]. This is also reflected in the fact that the Debye tem-

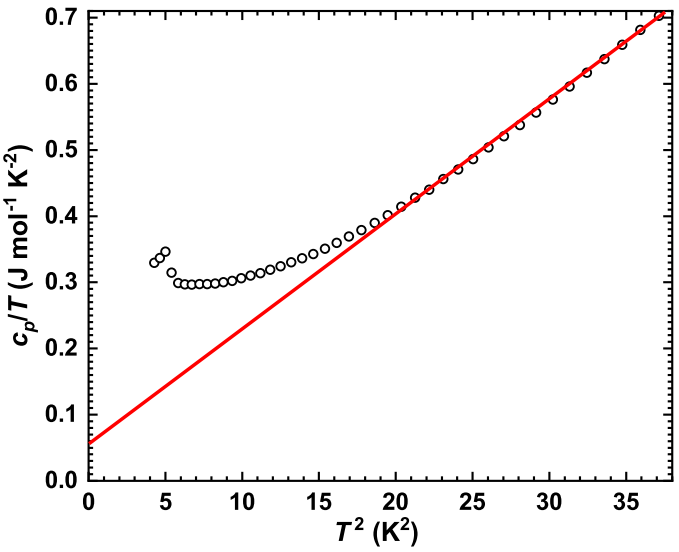

Fig. S4 Specific heat capacity for $Yb_5Rh_6Sn_{18}$ in $c_p/T(T^2)$ presentation together with the fit to the $c_p/T = \gamma + \beta T^2$ *ansatz* (red line).

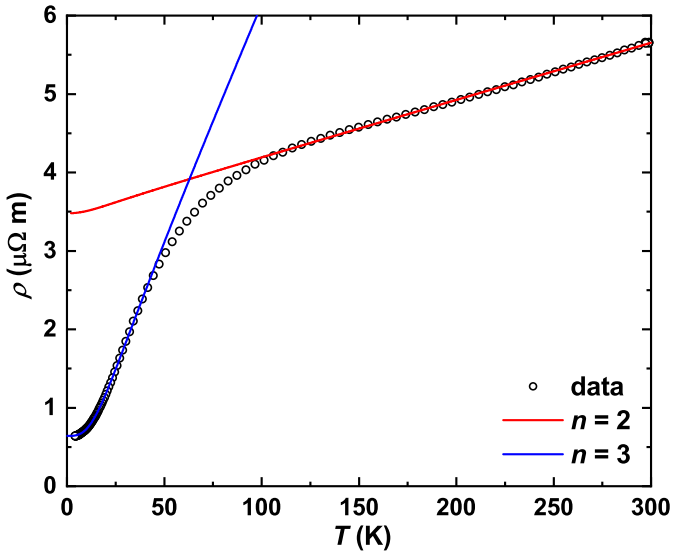

Fig. S5 Temperature dependence of electrical resistivity for $Yb_5Rh_6Sn_{18}$ together with the fits to Bloch-Grüneisen formula assuming different scattering mechanisms.

Table S1 Parameters from BG-fit of electrical resistivity of $Yb_5Rh_6Sn_{18}$.

Parameter	$n = 2$	$n = 3$
ρ_0, $\mu\Omega$ m	3.48(5)	0.64(1)
$A(\times 10^{-3})$, $\mu\Omega$ m	1.82(3)	28.6(1)
Θ_D^{res}, K	82(1)	96(1)

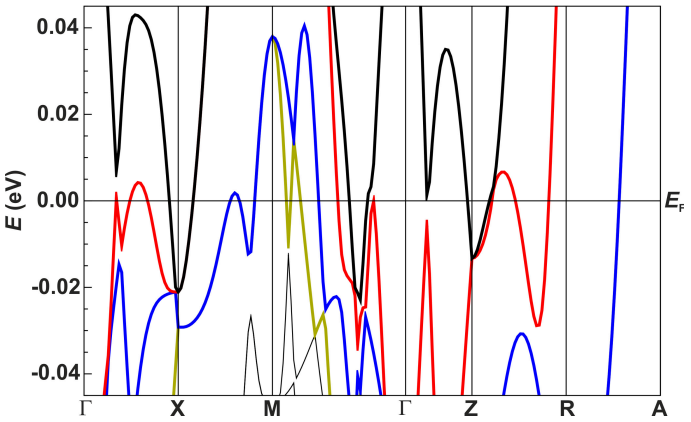

Fig. S6 Electronic band structure for $Yb_5Rh_6Sn_{18}$ in the close vicinity to the Fermi level E_F. Bands 617, 618, 619, 620 crossing E_F are given in light brown, blue, red, black colors, respectively.

peratures in Table S1 are by a factor of ≈1.5 smaller than Θ_D deduced from specific heat.

Table S2 Interatomic distances d at different temperatures in the crystal structure of $Yb_5Rh_6Sn_{18}$.

Atom	d, Å (200 K)	d, Å (293 K)
Yb1 - 4Sn2	3.398(2)	3.39(1)
- 8Sn4	3.417(2)	3.423(9)
- 4Rh2	3.495(2)	3.471(9)
- 2Rh1	3.531(2)	3.54(2)
Yb2 - 2Rh2	3.016(2)	3.023(9)
- 1Sn1	3.064(2)	3.04(1)
- 1Rh1	3.083(2)	3.05(1)
- 1Sn3	3.189(2)	3.15(1)
- 2Sn3	3.211(2)	3.216(9)
- 2Sn4	3.240(2)	3.24(1)
- 2Sn4	3.289(2)	3.28(1)
- 2Sn2	3.287(2)	3.29(1)
Rh1 - 4Sn4	2.640(2)	2.66(1)
- 2Sn3	2.734(3)	2.76(2)
Rh2 - 2Sn2	2.642(2)	2.63(1)
- 2Sn4	2.667(2)	2.64(1)
- 2Sn3	2.758(2)	2.76(1)
Sn1 - 2Sn2	3.119(3)	3.19(2)
- 2Sn3	3.622(2)	3.61(1)
- 4Sn4	3.623(2)	3.62(1)
- 4Sn4	3.894(2)	3.88(1)
Sn2 - 2Sn2	2.913(4)	2.93(2)
- 2Sn4	3.317(2)	3.32(1)
- 2Sn4	3.521(2)	3.50(1)
- 2Sn3	3.657(2)	3.62(1)
Sn3 - 2Sn3	3.324(3)	3.37(2)
- 1Sn3	3.352(3)	3.41(1)
- 2Sn2	3.657(2)	3.62(1)
- 2Sn4	3.680(2)	3.67(1)
- 2Sn4	3.705(2)	3.70(1)
Sn4 - 1Sn4	2.893(3)	2.87(1)
- 1Sn4	3.380(3)	3.41(1)
- 1Sn4	3.409(3)	3.42(1)

Notes and references

1 B. C. Sales and D. K. Wohlleben, *Phys. Rev. Lett.*, 1975, **35**, 1240–1244.

2 A. Grytsiv, D. Kaczorowski, A. Leithe-Jasper, V. Tran, A. Pikul, P. Rogl, M. Potel, H. Noël, M. Bohn and T. Velikanova, *J. Solid State Chem.*, 2002, **163**, 178–185.

3 M. Feig, L. Akselrud, M. Motylenko, M. Bobnar, J. Wagler, K. O. Kvashnina, V. Levytskyi, D. Rafaja, A. Leithe-Jasper and R. Gumeniuk, *Dalton Trans.*, 2021, **50**, 13580–13590.

4 R. Gumeniuk, R. Sarkar, C. Geibel, W. Schnelle, C. Paulmann, M. Baenitz, A. A. Tsirlin, V. Guritanu, J. Sichelschmidt, Y. Grin and A. Leithe-Jasper, *Phys. Rev. B*, 2012, **86**, 235138.

5 A. Hewson, J. Rasul and D. Newns, *Solid State Commun.*, 1983, **47**, 59–61.

6 M. Kasaya, F. Iga, M. Takigawa and T. Kasuya, *J. Magn. Magn. Mater.*, 1985, **47-48**, 429 – 435.

7 N. Mott and H. Jones, *The Theory of the Properties of Metals and Alloys*, Dover Publications, New York, 1958.

8 E. S. R. Gopal, *Specific Heat at Low Temperatures*, Plenum Press, 1966.